Tryptophan Dynamics of the FK506 Binding Protein: Time-Resolved Fluorescence and Simulations

Norberto D. Silva, Jr. and Franklyn G. Prendergast
Department of Pharmacology, Mayo Foundation, Guggenheim 1417, Rochester, Minnesota 55905 USA

ABSTRACT The FK506-binding protein (FKBP12) is important in the immunosuppressant action of FK506 and rapamycin. We have investigated Trp side chain dynamics in FKBP12, with and without a bound immunosuppressant, by measuring the Trp time-resolved fluorescence anisotropy decay $r(t)$. The $r(t)$ for W59 in aqueous uncomplexed FKBP12 at 20°C is well described by a single exponential with a recovered initial anisotropy, r_o^{eff}, of 0.192 and an overall rotational correlation time for the protein, ϕ_p, of 4.7 ns; $r_o^{eff} = 0.214$ and $\phi_p = 4.2$ ns for the FKBP12/FK506 complex. Using an expression for the order parameter squared, namely $S^2 = r_o^{eff}/r_o^T$, where r_o^T is the vitrified steady-state excitation anisotropy, we recovered an S^2 of 0.75 for W59 fluorescence in uncomplexed FKBP12 and $S^2 \approx 1$ in the FKBP12/FK506 complex. Results obtained for the FKBP12/rapamycin complex are similar to those found for the FKBP12/FK506 complex. Minimum perturbation mapping simulations were performed on the free and complexed forms of FKBP12 and the results were generally in agreement with the experimental data.

INTRODUCTION

The FK506-binding protein, FKBP12, is an important component in the immunosuppressant action induced by the drugs FK506 and rapamycin (Bierer et al., 1990; Clipstone and Crabtree, 1992; Schreiber, 1992). Both drugs invoke immunosuppression only after binding to FKBP12, and each complex leads to a different response (Sigal and Dumont, 1992; Schreiber and Crabtree, 1992). The FKBP12/FK506 complex binds and inactivates a Ca^{2+}/calmodulin-dependent protein phosphatase, calcineurin (Liu et al., 1991), which ultimately leads to arrest at the G0-G1 cell-cycle transition for the T cell through inhibition of the T-cell receptor signal transduction pathway. The FKBP12/rapamycin complex binds to a protein that is highly related to products of the DRR/TOR gene (Brown et al., 1994), and this leads to an inhibition of the interleukin-2 receptor pathway, thus preventing T-cell proliferation at the G1-S cell-cycle transition. Even though the above immunosuppressants inhibit the peptidyl-prolyl *cis-trans* isomerase (PPIase) activity of FKBP12 (Siekierka et al., 1989; Harding et al., 1989), it has been shown that PPIase inhibition does not account for the immunosuppressive action of the drug (Sigal and Dumont, 1992; Schreiber and Crabtree, 1992).

Given the encouraging immunosuppressant properties of FK506 relative to those of the less potent but traditionally used immunosuppressant cyclosporin A (Thomson, 1989; Starzl et al., 1990; Starzl, 1993), there has been and continues to be great interest in understanding the molecular mechanisms underlying the biochemistry of FKBP12—especially with regard to its interactions with immunosuppressant drugs. X-ray derived crystal structures are available for the FKBP12/FK506 complex (Van Duyne et al., 1991a), the FKBP12/rapamycin complex (Van Duyne et al., 1991b), the FKBP12/L-685,818 complex (Becker et al., 1993), the uncomplexed FKBP12 crystal structure (Wilson et al., 1995), and the FKBP12/FK506/calcineurin complex (Griffith et al., 1995); NMR-derived solution structures also exist for uncomplexed FKBP12 (Michnick et al., 1991; Moore et al., 1991). These data, however, fail to account for the possible effect of protein dynamics in ligand recognition, and there is reason to believe that such motions might contribute significantly to ligand binding (Yu, 1977; Munro et al., 1979; Frauenfelder et al., 1991; Rasmussen et al., 1992). Changes in FKBP12 dynamics upon ligand binding have been investigated by Cheng et al. in their ^{15}N NMR relaxation measurements of the protein's backbone (Cheng et al., 1993, 1994). They observed that the mainchain comprising residues 82–87, which forms a loop surrounding part of the ligand-binding site, becomes rigidly fixed upon FK506 binding to FKBP12 (Cheng et al., 1994).

To our knowledge there has been little study of the role of side chain dynamics on ligand binding. Yet, it seems apparent that side chain dynamics often do play a substantial role, and our lack of understanding may be the basis for the difficulty of many current attempts at structure based drug design (Verlinde and Dijkstra, 1995; Schevitz et al., 1995). Indeed, we would argue that a priori side chain interactions are principal determinants of the configuration of the binding site for many ligands. For example, a simulated drug-docking calculation conducted by our group for FK506 and rapamycin binding to FKBP12 suggests that these drugs will not interact with the protein when the docking simulation begins with the uncomplexed NMR solution structure; the drug docks perfectly, though, when the x-ray derived protein structure of complexed FKBP12 is employed (Pang et al., 1994). We believe the disparity derives from our

Received for publication 23 August 1995 and in final form 7 December 1995.

Address reprint requests to Dr. Franklyn G. Prendergast, Department of Pharmacology, Mayo Foundation, 200 First St., S.W., Rochester, MN 55905. Tel.: 507-284-4081; Fax: 507-284-9349; E-mail: prendergast@mayo.edu.

0006-3495/96/03/1122/16 $2.00

failure to properly consider side chain mobilities in the docking simulation.

The solitary Trp residue in FKBP12, W59, has been identified as essential for the interaction of FKBP12 with FK506 (Moore et al., 1991), although it is not obvious why. The fluorescence of this Trp residue changes upon drug binding, and this change has been used to monitor ligand binding (Marquis-Omer et al., 1991; Park et al., 1992) and protein stability (Egan et al., 1993). However, there has been little study of W59 dynamics despite the role its mobility could play in drug interaction. In this paper, we are concerned with the dynamics of W59. We have two objectives: First, we want to measure W59 mobility by use of time-dependent fluorescence anisotropy and to measure the fluorescence lifetimes, realizing that the latter may also be indicative of Trp side chain dynamics. Second, we are simulating W59 dynamics in an attempt to rationalize the fluorescence data. With regard to fluorescence lifetimes, for example, the prevailing interpretation of heterogeneous lifetimes invokes the existence of multiple Trp side chain conformations, i.e., the so-called rotamer model (Hutnik and Szabo, 1989; Rayner and Szabo, 1978), or alternatively a distribution of conformational substates (Alcala et al., 1987). Physical, or even theoretical evidence to corroborate these inferences is seldom presented (Harris and Hudson, 1990). At a minimum, a demonstration that more than one side chain conformation is feasible would be helpful. Furthermore a demonstration of possible interconversion between conformational states on the fluorescence time scale would also be valuable. To simulate Trp side chain dynamics we use the minimum perturbation mapping technique developed by Haydock (1993) from which an energy landscape for W59, as a function of its side chain χ_1, χ_2 dihedrals is calculated. In principle, molecular dynamics calculations could provide such insights, but the calculations are complicated by the length of time such simulations would have to run, i.e., into the nanosecond time frame. However, if we assume that the dynamical motions of W59 are solely determined by its χ_1, χ_2 dihedral, then minimum perturbation mapping allows us to consider the whole range of phase space.

METHODS

Expression and Purification of human FKBP12

Our purification procedure for human FKBP12 generally follows that described by Wiederrecht et al. (1992). *Escherichia coli* BL21 (DE3) competent cells (Novagen, Madison, WI) were transformed by plasmid pEThFKBP that was kindly provided by Dr. A. Marcy of Merck Research Laboratories. The transformed cells were then grown for 24 h on Luria-Bertani (LB) agar plates containing 100 μg/mL ampicillin at 37°C. This was followed by overnight growth of single colonies in 25 mL flasks of LB medium containing 100 μg/mL ampicillin at 37°C. One 25-mL culture flask was then used to inoculate 1 L LB containing 100 μg/mL ampicillin at 37°C in a shaker broth. When the culture optical density at 600 nm reached 0.5–0.6 (typically 2 to 3 h after inoculation) FKBP12 expression was induced by adding isopropyl β-D-thioglucopyranoside (IPTG) into the broth to a final concentration of 0.5 mM. The culture was then allowed to grow for another 10–11 h. After harvesting by ultracentrifugation and resuspension of the pellet twice in 20 mL 20-mM TRIS pH 7.4, the bacteria were stored overnight at −70°C and later thawed at room temperature. FKBP12 was released from the cell periplasm upon thawing and subsequently separated from unbroken cells and insoluble debris by ultracentrifugation. Thereafter, 1 mL 5% protamine sulfate was added to the resulting supernatant and stirred for 30 min at 4°C. The suspension was centrifuged and the resulting supernatant was concentrated to a volume of 9 to 10 mL, filtered and loaded onto a 175-mL Sephadex G-75 column containing a running buffer of 20-mM sodium phosphate, 50-mM Na_2SO_4, 1-mM ethylenediaminetetra acetic acid (EDTA) and 0.5-mM phenylmethylsulfonyl fluoride (PMSF). Collected fractions of FKBP12 were identified by SDS-PAGE, transferred to a 20 mM TRIS pH 8.0 buffer and concentrated to a volume of about 5 mL. The solution was then injected at 1 mL/min through a 5-mL HiTrap Q anion exchange column (Pharmacia Biotech, Uppsala, Sweden) that was equilibrated with 20-mM TRIS at pH 8.0. Purified FKBP12 came out in the void volume. The FKBP12 yield, using an extinction coefficient of 9860 M^{-1} cm^{-1} at 280 nm, was typically 18–20 mgs per liter of LB medium. The FKBP12 sample was then dialyzed extensively in 50-mM potassium phosphate buffer pH 7.0 and stored with 4-mM sodium azide at 4°C. We verified through SDS-PAGE and Coomassie blue staining that 1) FKBP12 was produced by the bacterial cells only after IPTG induction, and 2) negligible amounts of FKBP12 were left within the cell cytoplasm.

The fidelity of FKBP12 expression was verified by a sequence analysis of the first 39 amino terminus residues. The purity of the sample was also checked via HPLC by applying a 5 to 40% acetonitrile gradient over 69 min on a C-18 column (Applied Biosystems) from which was observed a single absorbance peak at 214 nm making up approximately 98% of the total signal area. In addition, the purity of the HPLC processed protein was verified using matrix-assisted laser desorption time of flight mass spectrometry (MALDI-TOF). HPLC fractions of FKBP12 were prepared for mass spectrometry by mixing the protein with a photoactive matrix, 3,4-dimethoxy-4-hydroxy-cinnamic acid and crystallizing the mixture on a steel target. A Bruker Biflex MALDI-TOF instrument (Bruker Instrument, Inc., Breman, Germany) was used in reflection mode to acquire the data. A single dominant charged peak was observed at m/z = 11821.5. The mass of this peak agreed well with 11819.5, the expected average molecular weight of FKBP12, and was within the 0.1% experimental error of the instrument. Finally, the protein PPIase activity was confirmed using an assay developed by Harrison and Stein (1990). The recovered k_{cat}/K_M for our purified FKBP12, using the Suc-Ala-Leu-Pro-Phe-pNA peptide (Bachem Bioscience, Inc., Philadelphia, PA) as a substrate, agreed closely with the literature (Park et al., 1992).

Immunosuppressant drugs

Immunosuppressant drugs FK506, kindly provided by Fujisawa Pharmaceutical Co., Ltd. (Osaka, Japan), and rapamycin (Biomol Research Laboratories, Plymouth Meeting, PA) were used without further purification. The immunosuppressants were weighed out with 10^{-5} g precision on a Mettler H51AR weigh balance and dissolved in high purity dimethyl sulfoxide (DMSO) from Burdick and Jackson (Muskegon, WI).

Absorption spectrum

The absorption spectra of uncomplexed FKBP12 and FKBP12 complexed with either FK506 or rapamycin were measured using a UV-VIS Cary 2200 spectrophotometer (Varian Techtron Pty, Ltd., Mulgrave, Australia). Data were taken at 0.2-nm intervals with a spectral bandwidth of 0.5 nm, a scan rate of 0.2 nm/s and a response time of 3 s. The spectral range covered 260–310 nm.

Steady-state fluorescence

Steady-state fluorescence spectral measurements were performed on a Perkin-Elmer MPF-66 fluorescence spectrophotometer (Perkin-Elmer,

Norwalk, CT) using 300-nm excitation (5-nm monochromator bandpass). The fluorescence emission was measured over the range 310–450 nm. During measurements all samples were kept at a temperature of 20°C. Whenever possible, the sample absorbance at 300 nm was kept around 0.1. This was not possible for the FKBP/rapamycin complex because of the high extinction coefficient of rapamycin (ϵ_{300nm} = 12,500 M^{-1} cm^{-1} in DMSO) in which case the fluorescence intensity was corrected for excitation inner filter effects (Lakowicz, 1983).

Low temperature steady-state excitation anisotropy measurements were performed on a Spex Flurolog spectrophotometer (SPEX Industries, Inc., Edison, NJ) equipped with a 0.22-m excitation monochromator and a Pelletier cooled photomultiplier tube. The emission was observed through an optical filter combination of UG1 (Melles Griot, Irvine CA) and two cut-on filters (WG345 and WG360) yielding half maximum transmittances at 357 and 384 nm. This optical arrangement minimized tyrosine fluorescence contributions to the excitation anisotropy. Filters were used for emission collection instead of the SPEX monochromator because of the unacceptably high g factors (≥3) associated with this monochromator; with filters, g factors of approximately 1 were obtained. The excitation range covered 270–310 nm in steps of 1 nm with a 3-s integration time. Only uncomplexed and FK506-complexed samples were considered, and both were dissolved in 66% (redistilled) glycerol:buffer mixtures at protein concentrations on the order of 100 to 200 μM.

Near-UV circular dichroism

Near-UV circular dichroism measurements of uncomplexed FKBP12 were performed at 20°C using a Jasco J-710 spectropolarimeter (Jasco, Tokyo, Japan). The sample was placed in a 0.5-cm pathlength cell at a concentration of 22 μM. The spectral range covered 250–320 nm using a 1.0-nm bandwidth.

Time-resolved fluorescence intensity and anisotropy decay

The Trp time-resolved fluorescence intensity and anisotropy decay of uncomplexed and complexed FKBP12 at 20°C were measured using time-resolved single-photon counting (O'Connor & Phillips, 1984). All samples were excited at 300 nm using the frequency-doubled output of a Coherent model 700 rhodamine dye laser that was pumped by the frequency-doubled output of a Coherent Antares YAG laser (Coherent, Palo Alto, CA). The fluorescence emission at 350 nm was observed through a 10-nm bandpass optical filter. Anisotropy decay measurements were performed by acquiring the time-dependent vertically and horizontally polarized fluorescence intensity decays ($I_{\parallel}(t)$ and $I_{\perp}(t)$, respectively), when excited by vertically polarized light, using a multi-channel plate detector. The instrument response function was recorded using a scattering solution, and it yielded a full width at half maximum of 50 ps; 3200–3600 channels were collected at 4.4 ps/channel using the Nucleus PCA-II data acquisition card (Oxford Instruments, Inc., Oak Ridge, TN). The protein concentrations for the time-resolved measurements were 200 μM for uncomplexed FKBP12 measurements, 50 μM for the FKBP12/FK506 complex measurements (with a 1.5-times molar excess of FK506 added), and 20 μM for the FKBP12/rapamycin complex measurements (with a 2.0-times molar excess of rapamycin added).

Data were analyzed using the Globals Unlimited program (Beechem & Gratton, 1988). The fluorescence intensity decay $I(t)$ was analyzed as a sum of decaying exponentials

$$I(t) = \sum_{i=1}^{N} \alpha_i \exp(-t/\tau_i) \quad (1)$$

with each ith term having lifetime τ_i and amplitude α_i. The fluorescence anisotropy decays were analyzed by fitting $I_{\parallel}(t)$ and $I_{\perp}(t)$ to the following expressions

$$I_{\parallel}(t) = (1/3)I(t)\,(1 + 2r(t)) \quad (2)$$

$$I_{\perp}(t) = (1/3)I(t)\,(1 - r(t)) \quad (3)$$

with the time-dependent anisotropy $r(t)$ given by

$$r(t) = r_o(S^2 + (1 - S^2)\exp(-t/\phi_w))\exp(-t/\phi_p)) \quad (4)$$

or

$$r(t) = r_o^{eff} \exp(-t/\phi_p) \quad (5)$$

where r_o in Eq. 4 and r_o^{eff} in Eq. 5 are the recovered initial anisotropies, S is the order parameter, ϕ_w is the rotational correlation time associated with the Trp residue motion and ϕ_p is the rotational correlation time of the protein molecule as a whole. Unless noted, all parameter errors were determined by the rigorous error analysis routine in the Globals Unlimited software using a confidence limit of 67%.

Typically, satisfactory fits of $r(t)$ to either Eqs. 4 or 5 are considered plausible if the recovered initial anisotropy is either close to the measured true initial anisotropy for free Trp (0.310 at 300-nm excitation), or if the value can be rationalized by an independent measurement of the true initial anisotropy r_o^T of the system in question. For the case where Eq. 5 yields a superior description for $r(t)$ we purposely denoted r_o^{eff} as an "effective" initial anisotropy if r_o^{eff} deviates significantly from r_o^T. We can still reason that r_o^{eff} is physically derived from r_o^T if in Eq. 4 we set $r_o = r_o^T$ and take $\phi_w \ll \phi_p$. As a result, Eq. 4 essentially reduces to Eq. 5, which is a single exponential having a pre-exponential factor of $r_o^T S^2$ that we denote as an effective initial anisotropy r_o^{eff} defined by

$$r_o^{eff} = r_o^T S^2 \quad (6)$$

Eq. 6 allows us to determine S^2 from parameters recovered in a fit to Eq. 5 provided we have some independent means of measuring the true initial anisotropy r_o^T. In our study, we determined r_o^T for Trp fluorescence in the protein by steady-state anisotropy measurements of the protein dissolved in a glycerol-water glass at −46°C (Valeur and Weber, 1977).

Theoretical calculations

Minimum perturbation mappings of W59 were performed using the CHARMM 22 executable code and specialized FORTRAN programs kindly provided by Dr. C. Haydock (Brooks et al., 1983; Haydock, 1993). Map calculations used the all-hydrogen CHARMM 22 parameter and topology file (Momany and Rone, 1992). Because the simulations placed FKBP12 in vacuum, ionizable residue charges were reduced by 80% and the dielectric constant was made numerically equal to the distance in ångstroms between interacting atoms to approximate solvent screening effects (Sharp, 1993). Nonbonded interactions were switched off over the range of 7.0 to 11.0 Å. In this work, even though we refer to a residue set to its crystallographic or NMR solution conformation, all FKBP12 structures in this study were conjugate gradient minimized for five steps to relax any energetically unfavorable bond lengths and atom overlap (the final structure generally differed by about 0.05 Å RMS from the initial structure).

The map starts out by fixing the Trp side chain at a particular χ_1, χ_2 point and setting all other residues to their crystallographic coordinates in the case of FK506 or rapamycin-complexed FKBP (Van Duyne et al., 1991a, b); for uncomplexed FKBP the coordinates of the 20 NMR solution structures were used (Michnick et al., 1991). Throughout this paper χ_1 is defined by the bond connectivity N-C_α-C_β-C_γ and χ_2 is defined by the bond connectivity C_α-C_β-C_γ-$C_{\delta 2}$. Then, for each Trp dihedral point, residues nearby Trp were allowed to conformationally relax so as to achieve energy minimization. The nearby residues included V24, Y26, F46, F48, V55, I56, E60, V63, L74, I76, F99 and V101. The resulting energy V was assigned as $V = V(\chi_1, \chi_2)$. The minimization procedure, used at each Trp dihedral point, was 40 steps by the steepest descent method, 280 steps by the Powell method and, with SHAKE (van Gunsteren and Karplus, 1980)

applied, 40 steps by the Powell method. This process is repeated in 5° or 10° steps over the whole angular space of χ_1 and χ_2.

Interconversion rates and order parameters were calculated from the maps according to previously discussed methods and are summarized as follows (Haydock, 1993). Based on transition state theory, in a two dimensional space, the interconversion rate k_{RP} from reactant R to product P is given by

$$k_{RP} = \frac{(2\pi/\beta)\omega^{-1}\exp(-\beta V(\chi_1^{\ddagger}, \chi_2^{\ddagger}))}{\int_{R_1}\int_{R_2}\exp(-\beta V(\chi_1, \chi_2))d_{\chi_1} d_{\chi_2}} \quad (7)$$

where $V(\chi_1^{\ddagger}, \chi_2^{\ddagger})$ is the potential energy at the transition state region, ω^2 is the positive eigenvalue resulting from a diagonalization of V about the transition state region (which is assumed to be quadratic), R_1 and R_2 denote the integration region defining the reactant state, and $\beta = 1/(k_B T)$ where k_B is Boltzmann's constant and T is the absolute temperature. In this work, we will consider the interconversion time from reactant R to product P, which is equal to $1/k_{RP}$.

The experimentally derived order parameter squared is customarily defined to depend on the rotations of the fluorophore relative to the protein, but not on the rotations of the transition dipole relative to the fluorophore. We approximately decouple the dipole and fluorophore rotations by expressing the calculated order parameter squared S_c^2 as

$$P_2(\cos(\delta))S_c^2 \quad (8)$$

$$\approx \frac{4\pi}{5}\sum_{mm'} Y_2^m(\theta_a, \phi_a)Y_2^{m'}(\theta_e, \phi_e)\sum_{m''}\langle D^{(2)}_{m''m}\rangle\langle D^{(2)}_{m''m'}\rangle$$

where P_2 is the second-order Legendre polynomial, δ is the angle between the absorption and emission transition dipoles, Y_2^m is the second-order spherical harmonic, θ_i and ϕ_i are the polar and azimuthal angles of the absorption ($i = a$) and emission ($i = e$) transition dipole in the fluorophore frame, and $\langle D^{(2)}_{mm'}\rangle$ is the ensemble average of the second-order rotation matrix element describing the transformation from the fluorophore reference frame to a frame attached to the protein. Integers m, m' and m'' range from -2 to $+2$. The above approximation for S_c^2 fails when δ is near the magic angle giving $P_2(\cos(\delta)) \approx 0$. Eq. 8 is the same as that derived by Haydock, except that his order parameter squared included the electronic dipole rotation, which is approximately removed by the $P_2(\cos(\delta))$ factor (Haydock, 1993).

If it is determined that the experimental anisotropy decay is best described by a single exponential decay, then S_c^2 determined by Eq. 8 can be compared to the experimentally derived order parameter squared S_e^2 via Eq. 6 through the relation $S_e^2 = r_o^{eff}/r_o^T$. This assumes that the fluorescence originates from a single emission transition dipole. When the fluorescence results from more than one emission transition dipole, then S_c^2 can be given by

$$S_c^2 = \frac{\sum_{i=1}^{N} f_i r_{oi}^T S_i^2}{r_o^T} \quad (9)$$

where N is the number of emission transition dipoles and f_i is the fractional intensity attributed to the ith emission transition dipole, which has a true initial anisotropy value of r_{oi}^T. S_i^2 is the order parameter squared derived through Eq. 8 from the ith emission transition dipole. A derivation of Eq. 9 is given in Appendix A; however, the main assumptions inherent in Eq. 9 are that 1) a single absorption transition dipole is exclusively excited in the system, and 2) the fluorescence intensity decay from each emission transition dipole is the same, save for a scale factor determined by the fractional intensity f_i. Once r_o^T is obtained the fractional intensities f_i can be determined for Eq. 9 by the equation.

$$r_o^T = \sum_{i=1}^{N} f_i r_{oi}^T \quad (10)$$

given that we assume some reasonable values for r_{oi}^T, which will be discussed more in the Results section.

RESULTS

Absorption spectrum

The absorption spectrum of uncomplexed FKBP12 in 50 mM-potassium phosphate buffer at pH 7.0 (data not shown) is typical of proteins bearing both Trp and Tyr residues (Wetlaufer, 1962). Upon addition of FK506 to yield a 1:1 protein-drug complex (whose stoichiometry was verified by observing W59 fluorescence quenching in a titration experiment), the absorption spectrum changes markedly (FK506 itself displays a relatively low extinction, and a subtraction of its absorption was implemented on the observed FKBP12/FK506 complex absorption). Prominent features of the FKBP12/FK506 complex absorption spectrum, relative to that of uncomplexed FKBP12, include a red shift of about 2 nm and increased spectral structure in the 280 and 290 nm regions. Indeed, N-acetyl-tryptophan-amide also displays the same qualitative absorption changes when it is transferred from an aqueous environment to a 90% dioxane/water mixture (data not shown), suggesting that the indole moiety of W59 is subject to decreased polarity upon ligand binding.

In the case of the FKBP12/rapamycin complex, a decomposition of the rapamycin absorption spectrum from FKBP12/rapamycin absorption spectrum could not satisfactorily yield an FKBP12 spectrum similar to the ones observed for uncomplexed or FK506-complexed FKBP12. In particular, the resulting decomposition tended to retain prominent features of the rapamycin absorption spectrum (data not shown), which include three peaks around 268 nm, 278 nm, and 292 nm attributed to the triene group of rapamycin. The strong extinction of rapamycin (i.e., 44,700 M^{-1} cm^{-1} at 280 nm) compared to uncomplexed FKBP12 (9860 M^{-1} cm^{-1} at 280 nm) is the likely reason for our inability to recover the FKBP12 absorption.

Steady-state fluorescence measurements

The W59 fluorescence spectrum of uncomplexed FKBP12 at 20°C, shown on Fig. 1 (*solid line*), displays an emission maximum (λ_{max}) at 330 nm. Qualitatively, the blue-shifted fluorescence spectrum of FKBP12, relative to aqueous Trp, indicates partial sequestration of the indole moiety from water, but no quantitative significance can be attributed to the term "partial sequestration." The water accessibility calculated from the NMR structures of uncomplexed FKBP yielded a range of 0 to 6 Å^2, which should be compared to the value of 210 Å^2 for free indole dissolved in water. Finally, the quantum yield of uncomplexed FKBP12, using aqueous Trp as a reference, is 0.014, which is about 10% of the value for free Trp in aqueous solvent (Demas and Crosby, 1971).

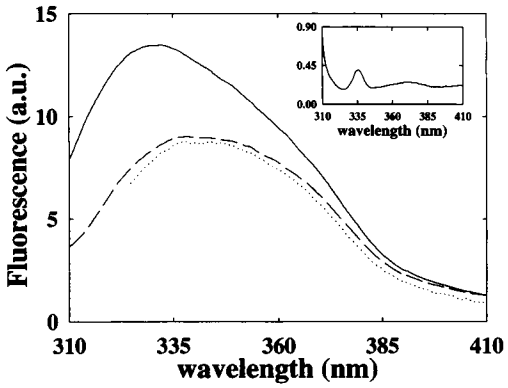

FIGURE 1 Fluorescence spectra, resulting from 300-nm excitation, of uncomplexed FKBP12 (*solid line*), FKBP12 complexed with FK506 (*dashed line*), and FKBP12 complexed with rapamycin (*dotted line*), which was corrected for the background fluorescence of aqueous rapamycin shown in the inset. All spectra are shown as a function of emission wavelength.

The dashed line curve of Fig. 1 shows the resulting fluorescence spectra of the FKBP12/FK506 complex in a 1:1 stoichiometry that displays a λ_{max} at 335 nm and decreased intensity relative to uncomplexed FKBP12. FK506 displays a solubility in water of about 70 μM (derived from the 620 M^{-1} cm^{-1} extinction of FK506 in DMSO at 300 nm), however no fluorescence was observed for aqueous FK506 when it was excited at 300 nm. As a result, the dashed curve of Fig. 1 is the resulting fluorescence of W59. Integrating over the emission spectrum shows that FK506 quenches the steady-state fluorescence of uncomplexed FKBP12 by 28%. We took advantage of the quenching of W59 fluorescence by FK506 to verify the 1:1 stoichiometry. Qualitatively, all of our observations are in accord with previous steady-state fluorescence measurements of W59 (Park et al., 1992; Marquis-Omer et al., 1991).

A fluorescence contaminant was observed for aqueous rapamycin with 300-nm excitation and its spectrum is shown in the inset of Fig. 1. We used the aqueous rapamycin fluorescence spectrum (rapamycin had an apparent aqueous solubility of about 27 μM) in the inset of Fig. 1 to subtract the background fluorescence of the drug from the fluorescence emission of the FKBP12/rapamycin complex. In addition, the resulting FKBP12/rapamycin complex fluorescence intensity had to be corrected for excitation inner filter effects because of the high extinction coefficient of rapamycin at 300 nm according to the method described by Lakowicz (1983). The 1:1 FKBP12/rapamycin complex fluorescence spectrum is shown as the dotted line of Fig. 1. Above 325 nm there is close agreement between this spectrum and that of the FKBP12/FK506 complex. Below 325 nm large Rayleigh scattering originating from the original background subtraction spectrum prevented a satisfactory spectrum of the FKBP12/rapamycin complex. Nevertheless, rapamycin quenches the steady-state fluorescence of W59 in FKBP12 by about the same amount as FK506 given the similarity between the two FKBP12 complexed spectrum.

Steady-state excitation anisotropy and near-UV CD

The absorption results of FKBP12 complexed with FK506 strongly suggest electronic interaction between W59 and FK506. This raises questions regarding the value for r_o^T to be used for calculations which led us to measure the excitation anisotropy profile of uncomplexed FKBP12 and FKBP12 complexed with FK506 in a 66% glycerol:water glass at −46°C. The fluorescence spectrum of uncomplexed FKBP12 and the FKBP12/FK506 complex in 66% glycerol at 20°C showed a 1–2 nm blue shift, relative to its aqueous spectrum. In other words, neither the uncomplexed FKBP12 nor the FKBP12/FK506 complex in 66% glycerol shows a substantially changed local electronic environment about W59, relative to that seen for the fully aqueous protein.

Fig. 2 shows the resulting low temperature (−45°C) steady-state excitation anisotropy of uncomplexed FKBP12 (*dashed line*) and the FKBP12/FK506 complex (*solid line*). The excitation anisotropy of uncomplexed FKBP12 shares similar features to the excitation anisotropy of Trp in propylene glycol at −58°C (Valeur and Weber, 1977). The main difference between uncomplexed FKBP12 and free Trp is the decreased magnitude of the excitation anisotropy of FKBP12 over the range 270–310 nm, relative to that of free Trp in a similar glass. For instance, the value of the uncomplexed FKBP12 anisotropy at 300 nm is 0.256, whereas for Trp it is 0.310 (Valeur and Weber, 1977). The observed difference in the low temperature anisotropy between free Trp and a single Trp protein or peptide has already been reported by Lakowicz et al. (1983). In fact, they recovered low temperature anisotropies at 300 nm in the range of 0.255 to 0.269, which is relatively close to the value we obtained for uncomplexed FKBP12. However, the excitation anisotropy of FKBP12 complexed with FK506 (*solid line* of Fig. 2) shows a much different excitation wavelength dependence than that observed for uncomplexed FKBP12. Of particular significance, is the decreased anisotropy value of 0.200 for the FKBP12/FK506 complex at 300 nm, relative to that of uncomplexed FKBP12.

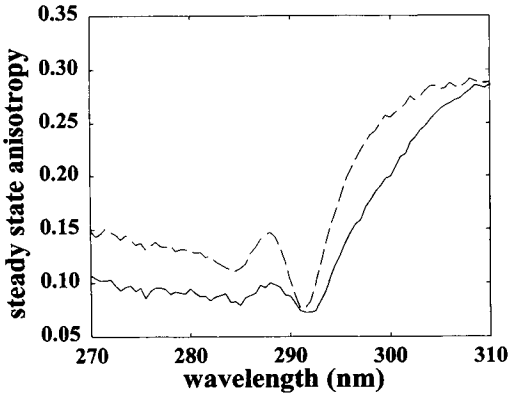

FIGURE 2 Excitation anisotropy of uncomplexed FKBP12 (*dashed line*) and FKBP12 complexed with FK506 (*solid line*) in 66% glycerol at −45°C as a function of excitation wavelength.

The excitation anisotropy spectrum of uncomplexed FKBP12 suggests that the aromatic residues closely circumscribing W59 may interact electronically to give a lower anisotropy value than that for free Trp in vitrified solution. To investigate this possibility we measured the near-UV CD of uncomplexed aqueous FKBP12 at 20°C and the resulting spectra (data not shown) show a distinct CD signal that includes two peaks at 280 and 287 nm having molar ellipticities of 25.7 and 42.8 deg cm^2 $dmol^{-1}$, respectively. This evidence is suggestive of aromatic residue interaction in FKBP12, though it is not sufficient to conclude specific aromatic residue interaction with W59.

Time-resolved fluorescence intensity and anisotropy decay

The W59 time-resolved fluorescence intensity decays of both uncomplexed and drug complexed FKBP12 at 20°C were best described by four fluorescence lifetimes (fits of the data to a distribution of lifetimes yielded unacceptably high χ^2). Table 1 shows the recovered values. For uncomplexed FKBP12, the lifetimes yield a fractional intensity weighted average lifetime, $\langle\tau\rangle$, of 3.3 ns that increases to 4.1 ns in the FKBP12/FK506 complex. The long lifetime component of both samples accounts for about 60% of the total intensity and also shows the greatest change after FK506 is bound to FKBP12—from 4.75 ns in uncomplexed FKBP12 to 5.43 ns in the complex. The magnitude of error in the lifetime components, determined from several repeated lifetime measurements, is ~5–7%.

The time-resolved fluorescence anisotropy decay of uncomplexed and FK506 complexed FKBP12 at 20°C was well described by a single rotational correlation time; adding a second rotational correlation time (i.e., Eq. 4) yielded essentially no change in χ^2. Fig. 3 shows the W59 time-resolved fluorescence anisotropy decay of uncomplexed FKBP12. Table 2 displays the recovered parameters for the W59 time-resolved anisotropy decay. The recovered overall rotational correlation times ϕ_p of 4.7 ns for uncomplexed FKBP12 and 4.2 ns in the FKBP12/FK506 complex closely agree with those predicted by the Stokes-Einstein relation (4.65 ns) for a spherical molecule of radius 16.5 Å, the latter being the approximate dimension of FKBP12 determined from NMR solution structures of uncomplexed FKBP12 (Michnick et al., 1991). For uncomplexed FKBP12, the recovered initial anisotropy r_o^{eff} of 0.192 is significantly lower than the measured low temperature anisotropy (0.256), excited at 300 nm. The FKBP12/FK506 complex yields a recovered initial anisotropy r_o^{eff} of 0.214 that, to within an experimental error of 5%, overlaps its low temperature anisotropy of 0.200 (error of 2%) at an excitation of 300 nm.

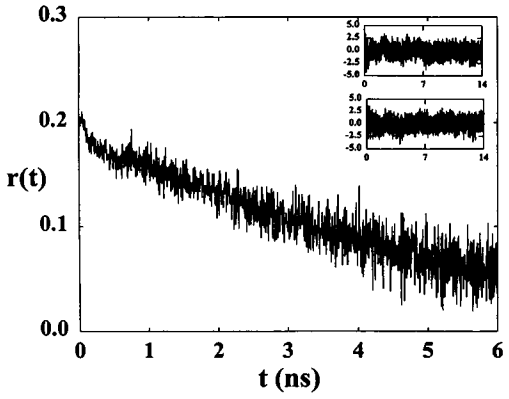

FIGURE 3 Calculated W59 fluorescence anisotropy decay of uncomplexed FKBP12 at pH 7.0 and 20°C as a function of time. The top and bottom insets show the residuals resulting from the data fit to the observed vertically and horizontally polarized fluorescence of uncomplexed FKBP12.

In the case of the FKBP12/rapamycin complex the fluorescence from rapamycin interferes with the measurement of the time-resolved W59 fluorescence of FKBP12. Consequently, we performed a background subtraction of the time-resolved fluorescence anisotropy decay of the FKBP12/rapamycin complex; that is, the vertically and horizontally polarized fluorescence emission decays of aqueous rapamycin were subtracted from the corresponding time-resolved polarized fluorescence emission of the FKBP12/rapamycin complex. Table 2 shows that we can get a satisfactory fit from the analysis (χ^2 of 1.1 with background subtraction versus 1.95 with no subtraction). More importantly the results are very similar to that of FKBP12 complexed with FK506. In particular, increases in r_o^{eff} and $\langle\tau\rangle$ are observed with respect to those of uncomplexed FKBP12. Indeed, the r_o^{eff} for the FKBP12/rapamycin complex is, to within experimental error, equal to that recovered for the FKBP12/FK506 complex. The recovered overall rotational correlation time of 4.9 ns also agrees closely with the previous results from uncomplexed FKBP12 and the FKBP12/FK506 complex.

SIMULATIONS

Uncomplexed FKBP12

Before proceeding, we must describe the nomenclature we employ to denote the putative configurational states which

TABLE 1 Fluorescence lifetime results: fluorescence amplitudes α_i and lifetimes τ_i

Sample	α_1	τ_1	α_2	τ_2	α_3	τ_3	α_4	τ_4	χ^2
FKBP12	0.09	4.75	0.08	1.95	0.26	0.29	0.57	0.10	1.2
FKBP12 + FK506	0.06	5.43	0.06	1.81	0.11	0.24	0.77	0.05	1.2
FKBP12 + Rapamycin*	0.10	5.24	0.14	2.25	0.12	0.44	0.64	0.07	1.1

*Analysis was done with background subtraction of rapamycin fluorescence.

TABLE 2 Time-resolved fluorescence anisotropy decay results

Sample	r_o^{eff}*	ϕ_p‡	$\langle\tau\rangle$§	χ^2¶	r_o^T‖	$S^2 = r_o^{eff}/r_o^T$**
W59 FKBP12	0.192	4.7	3.3	1.2	0.256	0.75
W59 FKBP12 + FK506	0.214	4.2	4.1	1.2	0.200	≈1.0
W59 FKBP12 + Rapamycin‡‡	0.218	4.9	3.7	1.1	—	—

*r_o^{eff} = initial anisotropy from time-resolved experiments. Errors are ± 5%.
‡ϕ_p = overall rotational correlation time in ns. Errors are ± 15%.
§$\langle\tau\rangle$ = Average fluorescence lifetime in ns obtained through fractional intensity weighted lifetimes.
¶χ^2 = reduced chi-square for anisotropy fit.
‖r_o^T = steady-state anisotropy obtained at low temperature and high viscosity. Errors are ± 2%. **S^2 = order parameter squared defined by $S^2 = r_o^{eff}/r_o^T$. Errors are ± 5% by propagation of errors.
‡‡Analysis was done with background subtraction of rapamycin fluorescence.

the Trp side chain can adopt. The χ_1 axis is partitioned into gauche-plus (g^+) for $0° < \chi_1 < 120°$, gauche-minus (g^-) for $-120° < \chi_1 < 0°$, and trans (t) for $120° < \chi_1 < 180°$ and $-180° < \chi_1 < -120°$. The χ_2 axis is also partitioned as perpendicular (p^+) for $0° < \chi_2 < 180°$ and antiperpendicular (p^-) for $-180° < \chi_2 < 0$. Thus, an isomer lying in one of six possible partition regions in χ_1, χ_2 space is categorized by two letters, the first of which signifies the χ_1 region of occupation and the second the χ_2 region.

Minimum perturbation map calculations of W59 in uncomplexed FKBP12 were performed on the NMR solution structure of uncomplexed FKBP12 deposited in the Brookhaven Protein Data Bank (Michnick et al., 1991). Even though two averaged NMR structures (PDB entries 1fks and 1fkt) of uncomplexed FKBP12 were deposited, in addition to the 20 NMR structures (PDB entry 1fkr) from which the averaged ones originate, our calculations concentrated on the latter structural set. We chose to do this because we did not want the conclusions drawn from our simulations to depend on any averaging algorithms from which the structures 1fks and 1fkt were derived; in particular, we believe confidence in our results will be enhanced by considering structures that have a direct association with the acquired data rather than those resulting from a post-processing of the final data. For our calculations we concentrated on the first NMR model of 1fkr. First we present W59 map calculations that essentially portray W59 to be surrounded by nearby residues, which themselves display little conformational flexibility. These calculations are then compared with W59 map calculations that incorporate substantial conformational flexibility for the nearby residues.

Fig. 4 *a* shows the W59 minimum perturbation map of uncomplexed FKBP12, and it predicts that state g^-p^+ for W59 has a Boltzmann-weighted probability of 0.99 at

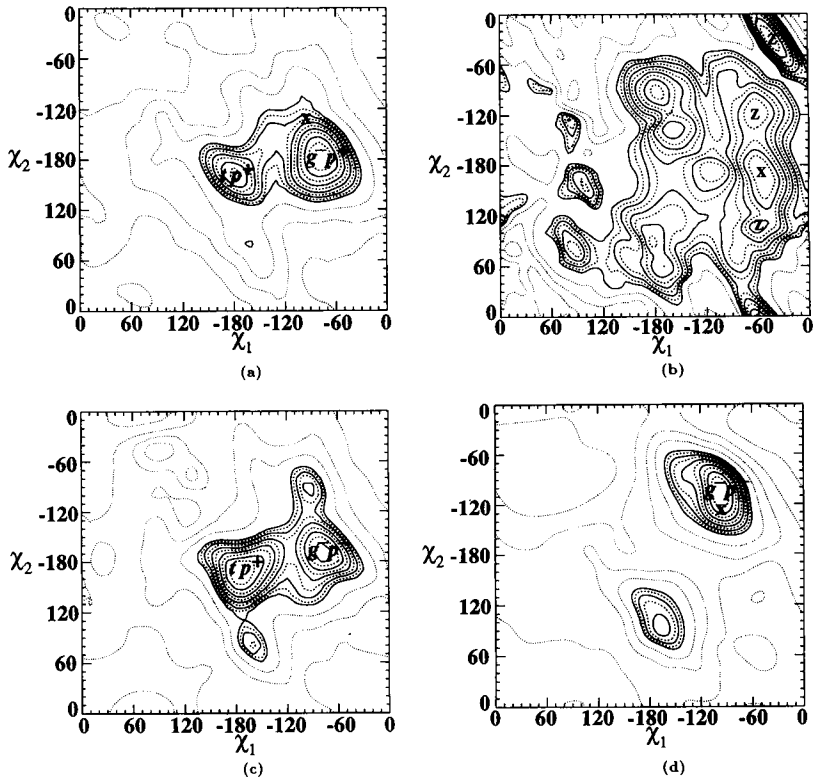

FIGURE 4 W59 minimum perturbation map of *a*) the first FKBP12 NMR model, *b*) Ala mutant structure of the first FKBP12 NMR model, *c*) the first FKBP12 NMR model with F48 and V63 isomerized to their secondary isomeric conformations; L50A and E50A mutations are also included, and *d*) FKBP12/FK506 complex with F48 and V63 isomerized to their secondary isomeric conformations; L50A and E50A mutations are also included. The maps are displayed as relative energy contour maps with the minimum (zero) energy coordinate indicated by g^-p^+ for *a*), x for *b*), tp^+ for *c*), and g^-p^- for *d*). The energy is in kcal/mol and the dashed contours indicate odd integer energy values (1, 3, 5, . . .); the solid contours indicate even integer energy values (2, 4, 6, . . .). Dotted contours indicate energies greater than 15 kcal/mol.

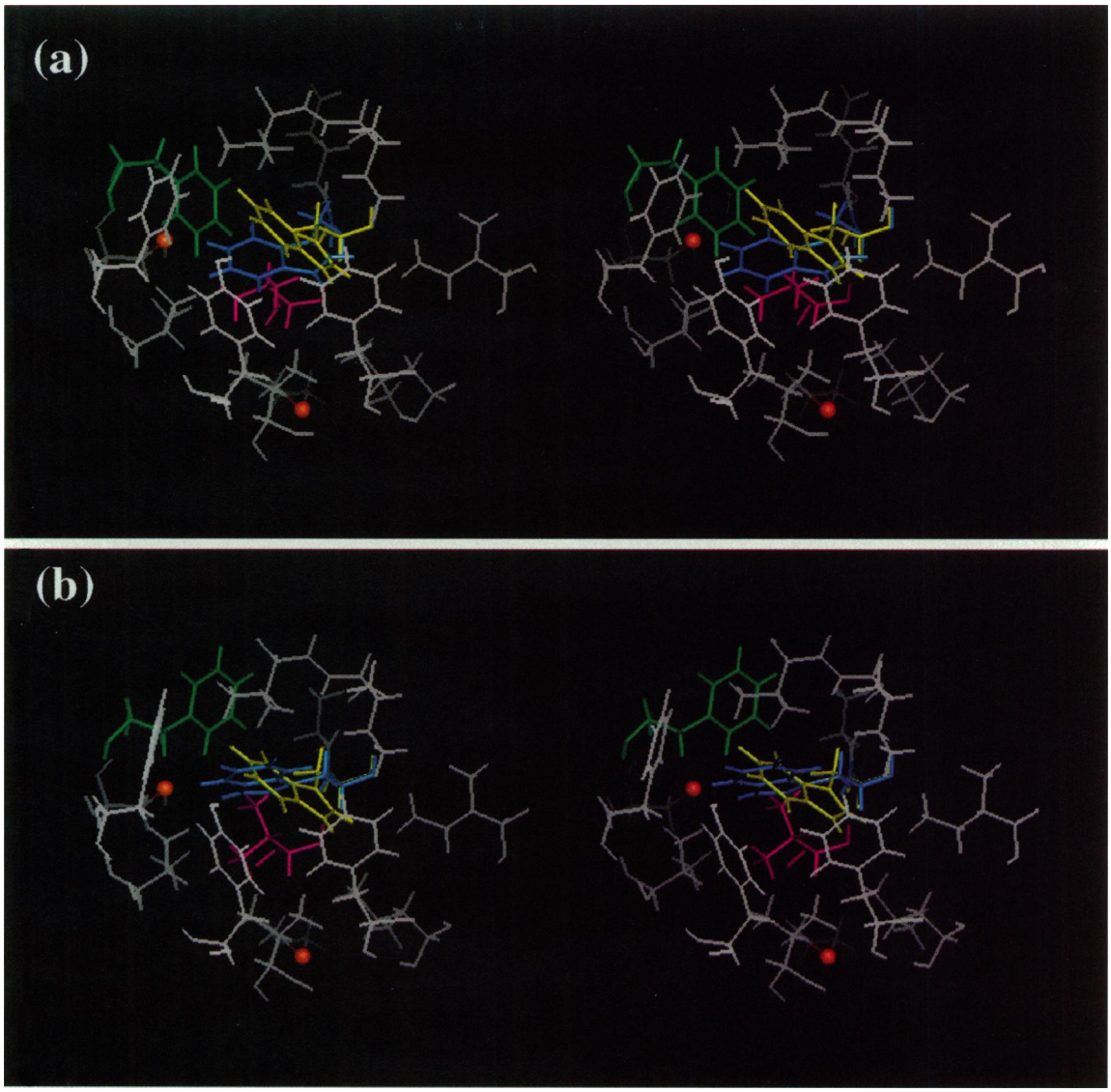

FIGURE 5 Stereo picture of region about W59 that includes nearby residues as defined in paper as well as C22 and M66 whose sulfur atom are emphasized as orange balls: *a*) W59 conformation obtained from the NMR structural data (*blue*) and predicted by a minimum perturbation map of W59 (*yellow*) using the same NMR structural data; the NMR solution structure of F48 (*green*) and V63 (*magenta*) are also emphasized. *b*) W59 isomers g^-p^- (*yellow*) and tp^+ (*blue*) as predicted from a W59 minimum perturbation map in which F48 (*green*) and V63 (*magenta*) are isomerized to their secondary isomeric conformations. The molecular graphics were done using the QUANTA program.

300K. However, this predicted W59 conformational minimum is different from the conformation given by the NMR solution structure, which is marked by **x** on Fig. 4 *a*. Fig. 5 *a* displays the discrepancy between the NMR solution structure of W59 in blue and the predicted W59 conformation from the map calculations in yellow. If we define the deviation of the predicted W59 minimum from the NMR W59 solution structure as being the Pythagorean distance between the two dihedral coordinates, we get a deviation of 56° for the case of the first NMR solution structure. A likely cause for the deviation noted in Fig. 5 *a* may derive from an inadequate solvent model. Another possible contribution to the deviation may be the inherently low resolution of the NMR structures. Nevertheless, the first NMR solution structure gives a relatively low deviation, in comparison with the other NMR models (calculations not shown), thus bolstering our confidence in using this structure as a basis for comparison with the experimental fluorescence data, because, to a relative extent, the map calculation satisfies structural constraints imposed by the NMR structural data.

The map calculations on the first NMR solution structure presented various predictions about W59 conformational heterogeneity and flexibility. For instance, in addition to the predominantly single isomeric state g^-p^+ of the W59 map in Fig. 4 *a*, another isomer, denoted by tp^+, was predicted with a low occupation probability of 0.01 at 300K. At this temperature, isomerization from state tp^+ to g^-p^+ would require an interconversion time of 47 ns, whereas the re-

verse direction had a interconversion time of 3 μs. Such long interconversion times, as compared to the average fluorescence lifetime of FKBP12, suggests a rather inflexible system on the nanosecond time scale. In addition, the relatively high inflexibility of isomer g^-p^+ can be characterized by its calculated order parameter squared S_c^2 using Eq. 8; for example, $S_c^2 \approx 1$ would imply a rigid system, whereas $S_c^2 \approx 0$ would suggest a flexible system. However, we must be careful as to how we calculate S_c^2 because it is dependent on what is assumed about the absorption and emission transition dipoles. In particular, the order parameter squared depends on the orientation of the absorption and emission transition dipole with respect to the chromophore; for simplicity, in this initial analysis, we assume that these transition dipoles lie in the plane of the indole ring. The absorption and emission transition dipole orientation angles, θ_a and θ_e, respectively, relative to each other determine the magnitude of the fluorescence anisotropy decay. Information about these orientation angles can be obtained by first knowing the true initial anisotropy r_o^T of the fluorophore and then applying the equation $r_o^T = 0.4P_2(\cos(\theta_a - \theta_e))$ to solve for θ_e, if θ_a is known. In our case, we measured an r_o^T of 0.256 at 300 nm for uncomplexed FKBP12. Using the above relation, our value of r_o^T would imply that the emission transition dipole is $\pm 29°$ relative to the orientation of the ^1L_a absorption transition dipole (Yamamoto and Tanaka, 1972). Assuming this as the origin for r_o^T such a model would predict an S_c^2 for state g^-p^+ of essentially 0.89 for either emission transition dipole orientation.

Alternatively, an $r_o^T = 0.256$ may be consequent to ultrafast intramolecular electronic processes involved in the conversion of the ^1L_a derived excited state to that derived from the ^1L_b transition dipole (Valeur and Weber, 1977). In particular, r_o^T may result from fluorescence emission polarized along the ^1L_a or ^1L_b transition dipole directions assuming that the ^1L_a dipole was exclusively excited at 300 nm. This would lead to r_o^T being given by the expression of Eq. 10; more explicitly, $r_o^T = f_A(0.4) + f_B(-0.2)$ where f_A and f_B are the fractional intensities arising from fluorescence emission polarized along the ^1L_a and ^1L_b directions, respectively. The factors 0.4 and -0.2 are the expected true anisotropy values for fluorescence emission resulting from the ^1L_a and ^1L_b directions, respectively, given that the ^1L_a transition dipole was excited. Thus, adopting 0.256 as r_o^T for W59 and incorporating electronic internal conversion as the origin for its value, fluorescence emission from uncomplexed FKBP12 would then result from both ^1L_a and ^1L_b states with fractional intensity weights of 0.76 and 0.24, respectively, at 300-nm excitation. This scenario, using Eq. 9, would yield an S_c^2 of 0.89 for state g^-p^+.

Even though recent experimental evidence has shown that Trp likely attains the theoretically maximum initial anisotropy of 0.4, this value decreases quickly, within 2 ps, via electronic internal conversion to approximately the 0.31 value obtained by Valuer and Weber (Ruggiero et al., 1990; Valeur and Weber, 1977). Thus, with respect to our experimental setup of 4.4 ps/channel and a full width at half maximum of 50 ps, it may only be relevant to consider r_o^T measured for FKBP12 in a highly vitrified environment. However, as noted by Bajzer et al., (1995) fluorescence lifetimes lower than the channel width may be obtained depending on the method used for discretization of the instrument response function. At present, our analysis uses the commonly implemented linear approximation (McKinnon et al., 1977). In conclusion, whether we consider the origin of r_o^T as being the result of electronic internal conversion or a $\pm 29°$ orientation of the emission transition dipole relative to the ^1L_a state, we obtain a high S_c^2 for the dominant g^-p^+ state.

Such high values of S_c^2 implies a relatively immobilized Trp side chain. In principle, the Trp side chain could exhibit increased mobility if residues nearby were allowed to isomerize away from Trp i.e., "collective" motions of nearby side chains could allow the Trp side chain to have several conformations. To get an idea of the full range of W59 conformational flexibility we have simulated side chain dynamics of residues near W59 by mutating them to alanine (Ala). Physically, the mutated structure portrays, relative to Trp, an average conformation in which thermal agitation induces large χ_1 dihedral rotations of a neighbor residue. We refer to this structure as the Ala mutant structure and its resulting map as the W59 Ala mutant map. We emphasize that the advantage of the W59 Ala mutant map is the ease with which we can approximate the mobility of residues neighboring the Trp side chain (reduced degrees of freedom and less atom-to-atom interactions to consider). The map serves as a starting point to explore the maximal range of Trp flexibility. Such a map may not portray reality with respect to a buried residue like W59. However, it at least points the way toward suggesting alternative regions of conformational space which Trp may occupy in addition to its conformation described by the NMR solution data.

We show in Fig. 4 *b* that many Trp isomers are energetically plausible for W59 in the Ala mutant structure with the most probable Boltzmann-weighted isomer labeled as **x**. If this map portrayed reality it would require a theoretical demonstration that the real residues nearby W59 can isomerize to conformations other than that given by the first NMR solution structure. However, minimum perturbation maps of nearby residues F99 and I56 showed that they cannot occupy isomeric states sufficiently different from those given by the NMR solution structure. In particular, the maps of F99 and I56 showed that these residues would have to overcome energy barriers greater than 10 kcal/mol to occupy very improbable isomeric conformations. Accordingly, we were reconciled always to include both residues in any further W59 map calculations. One consequence was that the inclusion of F99 or I56 into the Ala mutant structure (with their conformations given by the NMR solution structure) caused an elimination of the W59 isomers labeled **z** in Fig. 4 *b*. This prompted us to consider W59 isomers other than those labeled as **z** in Fig. 4 *b*. Consequently, our interest focused on the region of space where W59 is

proximal to residues F48 and V63. As before, we would only consider this region of conformational space as plausible for W59 if it could be shown that F48 and V63 could isomerize to conformations other than that given by their NMR solution structure. As it turns out, energetically favorable isomers of F48 at $\chi_1 = 170°$ and $\chi_2 = 90°$ was predicted from an F48 minimum perturbation map of an Ala mutant structure that included F46, W59, and F99 in their NMR solution coordinates and also included an additional Ala mutation of L50A. We denote such isomers, which are energetically favorable yet different from their given NMR solution conformation, as secondary isomers. A secondary isomer was also predicted for V63 at $\chi_1 = 85°$ from its map of an Ala mutant structure that included F46, W59, and F99 in their NMR solution coordinates. The secondary isomers for F48 and V63 were plausible since they were only separated from their NMR solution coordinates (the NMR solution coordinates for F48 is $\chi_1 = 72°$ and $\chi_2 = 108°$ and for V63 its $\chi_1 = -167°$) by energy barriers on the order of 5.5–7.5 kcal/mol. Thus, conformational flexibility of F48 and V63 suggested an alternative FKBP12 structure employing the secondary isomers of F48 and V63, which, as it turns out, allowed for increased W59 flexibility.

This increased W59 flexibility was verified by a W59 map, Fig. 4 *c*, of the first NMR solution structure which contained only two mutations, L50A and E60A, and two isomerizations of the nearby residues F48 and V63 to their secondary isomeric conformations. The L50A and E60A mutations model the average flexibility of L50 and E60 about their χ_1 dihedral so as to allow the isomerization of F48 to its secondary isomer. To first order, these mutations are plausible by the fact that L50 and E60 are relatively nonbulky residues on the protein surface. One of the predictions of this map is the existence of, at most, two isomeric conformations for W59. Both conformations are displayed in Fig. 5 *b*. One isomer, g^-p^-, that has a 0.07 occupation probability at 300K and is colored yellow in Fig. 5 *b*, is close to g^-p^+ observed in the W59 map of Fig. 4 *a*. The other, tp^+, is colored blue in Fig. 5 *b* and it is attainable from g^-p^- in an interconversion time of 3 ns; the reverse interconversion time is 42 ns. With or without electronic internal conversion, the S_c^2 of these isomers range from 0.89 to 0.94. We can also calculate the combined order parameter squared of both isomeric states. In particular, with no electronic internal conversion and an emission transition dipole angle of $-10°$, we obtain a combined S_c^2 of 0.79. If we apply electronic internal conversion, then the combined S_c^2 becomes 0.74.

Complexed FKBP12

Even though crystallographic structures were provided for complexed FKBP12 (for the case of the FKBP12/rapamycin complex, residues I90 and V98 had two possible conformations listed as structure A or B in PDB file 1fkb; we used structure A), the difficulty we faced in this part of the study was assigning appropriate parameters to the immunosuppressants FK506 and rapamycin. As mentioned by Fischer et al. (1993) and Orozco et al. (1993), care must be taken when assigning the force field parameters to the proline residues of peptides that can be isomerized by FKBP12. In particular, standard parameters do not accurately model the proline residue when it experiences large deviations from the *cis* or *trans* states. This caveat is probably relevant to the immunosuppressants, because both drugs contain a pipecolinyl ring that can be viewed as a proline analog in its transition state between *cis-trans* isomerization (Albers et al., 1990).

Given our uncertainty in the parameters of the whole drug we opted for a conservative approach. That is, we generated CHARMM parameters for the drugs using the QUANTA program (Molecular Simulations, Inc., Burlington, MA). In the parameter generation a total charge of zero was smoothed over all drug atoms. Then in the minimum perturbation maps of complexed FKBP12 all drug atoms were fixed. A more rigorous study would allow the drug atoms to adjust position, provided that justifiable parameters are known. We are currently working on the parameter assignments for FK506 so that such a study can be conducted in the future. Even though our present approach may be considered a first order approximation, it should be noted that NMR relaxation measurements of FK506 bound to FKBP12 indicates that the drug macrocycle backbone is relatively immobile on the picosecond time scale (Lepre et al., 1993). Thus, there is at least some experimental basis for our modeling of FK506.

In our simulation, because the drug is bound "on top" of W59 and is fixed during minimization, only a single dominant state can result from the W59 map. This raises the question whether there is any value in a W59 map using a model in which the drug is fixed. To answer this question we did a control W59 map in which all of the neighboring residues of the FKBP12/FK506 complex were mutated to Ala. The resulting map (not shown) verifies the possible existence of multiple isomeric states for W59 though not as many as in the W59 Ala map of Fig. 4 *b*. Thus, if flexibility is possible for the nearby residues in complexed FKBP12, then W59 might also demonstrate some flexibility in the FKBP12/FK506 complex.

However, as we have demonstrated in the uncomplexed case, the Ala mutant structure is not the correct model to use when trying to portray FKBP12 motional flexibility of residues nearby W59. Rather only the isomerizations of F48 and V63 to their secondary isomers could be justified. Applying these isomerizations as well as the L50A and E60A mutations to the protein in the FKBP12/FK506 complex yields the W59 map of Fig. 4 *d*. The map clearly displays less flexibility for W59 than the corresponding map in Fig. 4 *c* of uncomplexed FKBP12. In particular, only a single minimum, state g^-p^-, is observed for W59. This minimum is close to the observed (measured) dihedral coordinates, labeled **x** in Fig. 4 *d*, of W59 from the crystallographic structure of the FKBP12/FK506 complex.

For our calculations of S_c^2 we use the experimentally determined r_o^T of 0.200 obtained from the low temperature-high viscosity measurements of the steady-state fluorescence anisotropy of the FKBP12/FK506 complex. With no electronic internal conversion, state g^-p^- gives an S_c^2 of 0.88 or 0.92 for $\theta_e = -5°$ and $\theta_e = -75°$, respectively. With electronic internal conversion, an S_c^2 of 0.90 is calculated where the ^1L_a absorption transition dipole contributes approximately 0.66 of the fractional intensity. A map similar to that of Fig. 4 *d* was recovered for the W59 map of the FKBP12/rapamycin complex.

DISCUSSION

Proteins containing a single Trp residue display heterogeneous fluorescence intensity decays requiring a description in terms of two or more fluorescence lifetimes (Beechem and Brand, 1985). A variety of quenching mechanisms apparently influence the nonradiative decay of excited-state Trp. These mechanisms include charge transfer, resonance energy transfer, proton transfer, and intersystem crossing (Shizuka et al., 1988; Janes et al., 1987; Saito et al., 1984). With the exception of resonance energy and electron transfer, the deactivation mechanisms involve collisional interaction between the indole moiety and the quenching residue. Two views rationalizing the observed heterogeneity in the fluorescence intensity decay have emerged over the years. The first view involves a "rotamer" model and purports that each lifetime component, which results from a fit of the intensity decay to a finite number of exponentially decaying terms, is due to a particular Trp isomer (Hutnik and Szabo, 1989; Rayner and Szabo, 1978). From this model, different lifetime values are due to the indole moiety being in collisional contact with different moieties having differing quenching efficiencies. The second rationalization for fluorescence lifetime heterogeneity proposes the existence of conformational substates (Alcala et al., 1987; Frauenfelder et al., 1988). This model holds that the protein's energy landscape is multidimensional, and, as a result, a continuous distribution of Trp fluorescence lifetimes arises from both a multitude of Trp isomers and different rotational isomers of nearby quenching residues.

For the study of Trp fluorescence described here, the principal issue is that all FKBP12 samples displayed a complex heterogeneity in their W59 fluorescence intensity decays as evident in the four lifetime components needed to describe the experimental data. The fact that uncomplexed FKBP12 shows a low quantum yield of 0.014, which is about 10% of that found for free Trp in aqueous solution (Demas and Crosby, 1971), clearly indicates substantial quenching of W59 fluorescence. Yet, despite the extensive quenching evident in the reduced quantum yield, long lifetime components (i.e., where $\tau > 4.0$ ns) persist indicating the complexity of the quenching processes. The identities of the latter are unclear. We assume that elements in the protein matrix are primarily responsible and the possibility of static versus dynamic quenching may also need to be considered. However, the term "static quenching" as it may be applied here within the commonly used lexicon is particularly unsatisfying. It becomes little more than a catch all phrase to describe but not explain the results. The truth is we do not know the basis for the recovered lifetimes yet the pattern found in this work, namely low quantum yield and a set of long τ values is very common (Sedarous and Prendergast, unpublished results). To the extent that we can trust the recovery of parameters then the results must be considered as "real." If so, then our usual explanations fail precisely because we cannot identify the quenching mechanisms. Examination of the molecular environs of W59 and of the near-UV CD spectrum for the protein suggests the possibility of some ground-state electronic interaction but these are not quantifiable. We also do not fully understand what the consequences of such interactions would be on the excited state decay although in general we would guess an inevitable reduction in quantum yield and shortening of the fluorescence lifetime. Beyond this consideration, examination of the residues immediately surrounding W59 shows no obvious collisional quenching groups such as charged moieties or sulfur containing residues (Steiner and Kirby, 1969; Harris and Hudson, 1990).

Upon complexation the fluorescence quantum is reduced further to $\approx$0.01 and the fluorescence emission red shifts (Park et al., 1992). This spectral shift to the red and the fluorescence quenching by drug binding are interesting results. Calculations show that drug-bound protein has a water accessibility for W59 of zero. Yet, commonly held views would predict "moderate" water accessibility given the W59 fluorescence maximum of 335 nm. As for the quenching, in both drug complexes with FKBP12 only the pipecolinyl ring directly interacts with the indole moiety, as shown in Fig. 6. Beyond this structural coincidence between the two drugs there is no obvious explanation for the observed quenching upon drug binding.

Another result of drug complexation is the increase of $\langle\tau\rangle$, which agrees qualitatively with that observed for the FK520-FKBP12 complex (Marquis-Omer et al., 1991). However, the $\langle\tau\rangle$ of 2.1 ns obtained for uncomplexed FKBP12 by Marquis-Omer et al. (1991) was a least a nanosecond shorter than ours. The origin of this difference is not obvious. However, in their study, FKBP12 was excited at 292 nm and the fluorescence signal measured may have been contaminated by tyrosine emission. Nevertheless, the increase in $\langle\tau\rangle$ contrasts obviously with the ligand-induced decrease in quantum yield. A possible explanation for this discrepancy may reside in a change in the radiative lifetime of Trp after the ligand is bound. This change is plausible considering that Trp may display a wide range of radiative lifetimes in a variety of proteins (Szabo and Faerman, 1992). However, it is not obvious how to derive a system's radiative decay rate when its decay is multiexponential, as the case is with FKBP12; our caution in this matter is discussed in Appendix B.

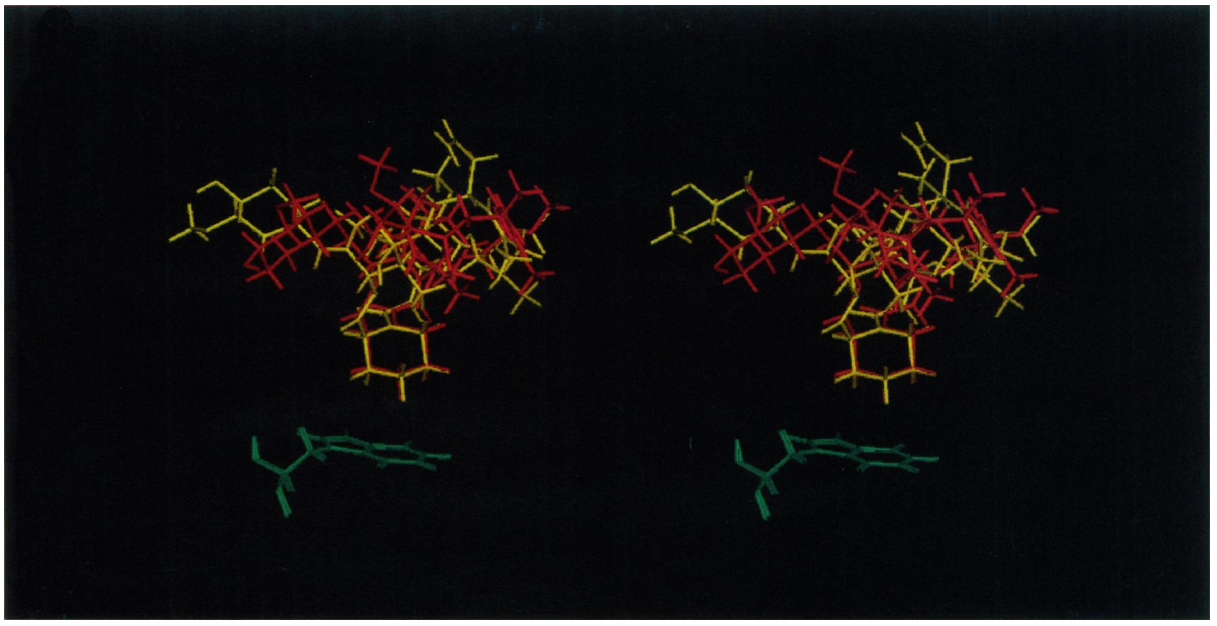

FIGURE 6 Stereo picture of W59 (*green*) and the FK506 (*yellow*) and rapamycin (*red*) drugs resulting from a superposition of the x-ray derived crystal crystal structures of the FKBP12/FK506 and FKBP12/rapamycin complex. Hydrogen atoms were added on by the CHARMM program and the molecular graphics were done using the QUANTA program.

Despite the difficulty we have in identifying the interactions responsible for quenching, it is desirable to probe the possible existence of multiple conformations for the Trp side chain, i.e., the likelihood of credible "rotamers." Our simulations of FKBP12 show that two W59 isoforms can be rationalized in the case of uncomplexed FKBP12 and only one in the case of the complexed FKBP12 (Fig. 4, *c* and *d*). Thus, from both experimental and theoretical approaches the Trp rotamer model as a source for the lifetime heterogeneity does not seem practicable if collisional mechanisms are the primary mechanism of quenching. Plausible isomerizations of W59 and combinations of isomerizations of nearby residues like V63, F48, V55 and V101 (V55 and V101 were also shown to exhibit secondary isomers from our simulations, data not shown) may coexist and could give rise to a multitude of lifetimes were it not for the fact that all residues nearby W59 are very weak quenchers, if they quench at all. In general, these paradoxical changes in quantum yield and fluorescence lifetimes, the manifest heterogeneity in fluorescence intensity decays and the absence of obvious structural basis for these fluorescence properties suggests that we may have paid insufficient attention to quenching mechanisms that are not collisional, i.e., those operating through space (Bajzer and Prendergast, 1993). Finally, what must be realized is that it really does not matter whether we interpret the heterogeneity of lifetimes in terms of discrete exponentials or distributions. The use of four exponentials terms is a consequence of the fitting procedure and the results are fully reproducible, but the physical meaning of the recovered parameters is clearly problematic. Three exponential terms do not fit well; five may be marginally better than four. The key issue is the complexity of the decay and the apparent inadequacy of any single model, rotamer-based or distribution of states, to simply interpret the results.

Given the previous conclusions of the limited conformational states W59 can occupy, what can be concluded of the motions of W59 and its relevance toward drug binding? In this respect, our study presents two major implications vis-à-vis W59 motion that we now discuss.

Traditionally, a double exponential decay (Eq. 4) is used to describe Trp motion if there is reason to believe the motions implied actually exist. In the case of uncomplexed FKBP12, the χ^2 of a double exponential fit is essentially equivalent to a single exponential fit (Eq. 5) and, thus, the latter is the preferred fit. The single exponential portrayal of $r(t)$ for W59 in uncomplexed FKBP12 suggests that the Trp residue is rigidly "fixed", i.e., the experimentally derived S^2 should be 1.0. This would clearly be the case if we could fit $r(t)$ to a single exponential with r_o^{eff} fixed either to the r_o^T of free Trp or that determined for W59 in uncomplexed FKBP12 by our low temperature steady-state anisotropy measurements. However, in either case the resulting fits yielded an inferior χ^2 (>3).

This leads to an alternative explanation for the relatively low $r_o^{eff} = 0.192$ value of W59 for uncomplexed FKBP12; that is, it results from a double exponential decay representation of $r(t)$ in which r_o of Eq. 4 is the r_o^T value of 0.256, and $\phi_w \ll \phi_p$ holds such that Eq. 4 reduces to the single exponential expression of Eq. 5 where $r_o^{eff} = r_o^T S^2$. In other words, if we were to freeze the sample and measure its time-resolved anisotropy decay, the motion of W59 should be slowed down such that an initial anisotropy of 0.256 would be recovered. Indeed, at 20°C, we can fit the anisot-

ropy decay to Eq. 4 with r_o fixed to 0.256 and get a ϕ_w of 9 ps, ϕ_p of 4.8 ns and an S^2 of 0.74. However, such a fit would yield an error on ϕ_w on the order of 100% because its χ^2 is equivalent to that of a single exponential decay fit. Nevertheless, we can still adopt the single exponential fit by appealing to a fast W59 depolarization that yields an S^2 of 0.75 for uncomplexed FKBP12 using $S^2 = r_o^{eff}/r_o^T$.

A similar line of argument rationalizing the use of a single exponential decay for describing the anisotropy decay of drug-complexed FKBP12 also applies. In particular, the 0.200 value of r_o^T and the recovered r_o^{eff} of 0.214 for W59 in the FKBP12/FK506 complex, are equal within experimental error, which implies an absence of W59 side chain motion, giving $S^2 \approx 1.0$ for W59 in the FKBP12/FK506 complex. With respect to rapamycin effects, because 1) close similarity between the steady-state fluorescence emission spectrum of the FKBP12/rapamycin complex and that of the FKBP12/FK506 complex exists, and 2) similar changes in the recovered r_o^{eff} and $\langle\tau\rangle$ of both complexes relative to that obtained for uncomplexed FKBP12 exist, we believe that our results suggest an $S^2 \approx 1$ for W59 in the FKBP12/rapamycin complex. Thus, the first major implication of this study is that the side chain dynamics of W59 may be an important factor in the ligand binding of immunosuppressants FK506 and rapamycin to FKBP12.

Given the previous experimental facts, the S_c^2 calculated from the W59 map of uncomplexed FKBP12 agrees with the experimental S^2 only if we assume that residues near W59, namely F48 and V63, can readjust to their secondary isomers. In particular, an S_c^2 of $\sim 0.74-0.78$ resulted when we combined states tp^+ and g^-p^- in the map of Fig. 4 *c*, which agrees closely with the experimentally recovered S^2 of 0.75. Combining states tp^+ and g^-p^- assumes that the interconversion time between the two states is short compared with the average fluorescence lifetime. Because of the relatively large interconversion times between the two states (3 ns and 47 ns) one would expect that a discernible ϕ_w value should be observed from the fluorescence anisotropy decay of W59. This discrepancy may have its origin in the way we modeled solvent effects on the map. Yet, use of a more appropriate solvent model could completely change our calculated S^2, because the latter is derived from a Boltzmann-weighted average as described in Eq. 8. Finally, our calculations show the S_c^2 of the combined states tp^+ and g^-p^- for uncomplexed FKBP12 increases from ~ 0.74 to ~ 0.90 after FK506 is bound. Experimentally we see a similar increase in S^2 from the uncomplexed value of 0.75 to the complexed value of ~ 1.0. Overall, the simulations are in qualitative accord with experiments in that the order parameter of W59 increases after drug binding. Thus, the second major implication of our study is that we can rationalize the observed fluorescence anisotropy decay of W59 through molecular simulations to give us a first order insight into the mechanisms of W59 motion.

Considering that the drugs effectively increase the packing density directly above the indole ring in the FKBP12-drug complex (Van Duyne et al., 1991a, b), our experimental and theoretical results are physically consistent with the implication that such a sequestering by the drugs would restrain the mobility of W59. In addition, the calculated average B-factor $\langle B\rangle$ of all heavy atoms for W59 supports this notion for decreased W59 mobility in the protein-drug complexes. $\langle B\rangle$ for W59 heavy atoms is 14.9 for uncomplexed FKBP12 (private communication, Dr. B. McKeever, Merck Research Laboratories, Rahway, NJ) but is only 7.6 in the FKBP12/FK506 complex (Van Duyne et al., 1991a). Even though the uncomplexed and FK506-complexed structures were derived from different crystal symmetry forms, their $\langle B\rangle$ for all protein heavy atoms are relatively similar with 14.9 for the uncomplexed structure and 13.7 for the FK506-complexed structure. The x-ray data for both crystal structures were acquired at similar temperatures. Such similarity suggests that our comparison of $\langle B\rangle$ for W59 heavy atoms is plausible.

Although our results agree qualitatively with changes of $\langle B\rangle$ for W59, there is a major difference in the recovered overall protein rotational correlation times determined by fluorescence and NMR. The NMR relaxation measurements yielded a τ_m, which corresponds to ϕ_p of Eq. 4, of 9.2 ns for uncomplexed FKBP12 and 9.0 ns for the FKBP12/FK506 complex (Cheng et al., 1993, 1994). These values are almost a factor of two greater than our ϕ_p values of 4.7 ns for uncomplexed FKBP12 and 4.2 ns for the FKBP12/FK506 complex. The NMR and fluorescence measurements were both done in a 50-mM potassium phosphate buffer composition and at pH 7.0. Whereas our measurements were performed at 20°C and the NMR relaxation measurements were done at 30°C, this difference is not sufficient to account for the observed differences in ϕ_p. Discrepancies between the NMR relaxation τ_m and the time-resolved fluorescence anisotropy ϕ_p have been observed in other studies investigating the side chain dynamics of Trp and Tyr residues (Kemple et al., 1994; Palmer et al., 1993) and there are as yet no convincing explanations.

Our results suggests the need for future studies with respect to W59 side chain dynamics. The simulations suggest that the origin of W59 motion is predominantly along χ_1, if one assumes that the W59 anisotropy decay is determined primarily by its side chain dihedral motions rather than by "breathing" motions of the peptide backbone or electronic effects. The model predicts ways of testing for these motions. In particular, site-directed mutagenesis of F48 or V63 may influence the observed anisotropy decay of W59. Further analysis also suggests that V101 may be interesting for mutagenesis studies, because it may sterically hinder W59 and so may determine the barrier height between states tp^+ and g^-p^- of Fig. 4 *c*. In addition, our study suggests a way to improve drug association with FKBP12. Assuming that, from the crystal structure of the FKBP12/drug complex, the W59 isomer g^-p^- of Fig. 4 *c* is preferred over tp^+ for drug association, improved drug interaction may be affected by site directed mutagenesis of residues determining the conformational freedom of W59 as implied by isomer tp^+.

This work was supported in part by the Mayo Foundation, by grant GM 34847 (to FGP) and by the Cancer Research Fund of the Damon Runyon-Walter Winchell Foundation Fellowship, DRG-1289 (to NS). Thanks are expressed to Dr. A. Marcy and Dr. B. McKeever of Merck Research Laboratories for providing the human FKBP12 plasmid and the crystal coordinates of uncomplexed human FKBP12. Thanks also to Dr. T. Felmee, Dr. D. Braddock, Dr. C. Haydock, Dr. Y-P. Pang, Ms. S. Kurian, Dr. W. Kirk, and Mr. T. Wieand for their technical advice.

APPENDIX A

On the order parameter of a fluorescent system having multiple emission transition dipoles

Fluorescence anisotropy decay data are fit to $I_{\parallel}(t)$ and $I_{\perp}(t)$ of Eqs. 2 and 3 and not directly to $r(t)$. What follows is a derivation of Eq. 9 by considering $I_{\parallel}(t)$ although a similar derivation can also be applied to $I_{\perp}(t)$.

Assuming that fluorescence emission from a fluorophore originates from N emission transition dipoles labeled by i after a single absorption dipole is excited, $I_{\parallel}(t)$ can be decomposed as

$$I_{\parallel}(t) = \sum_i I^i_{\parallel}(t) \tag{11}$$

where $I^i_{\parallel}(t)$ is the vertically polarized fluorescence emission resulting from the ith emission transition dipole; it is understood throughout this appendix that all summations range from 1 to N.

Equation 11 can then be rewritten as

$$I_{\parallel}(t) = (1/3)\sum_i I^i(t)\,(1 + 2r_i(t)) \tag{12}$$

where $I^i(t)$ and $r_i(t)$ are the fluorescence intensity and anisotropy decay associated with the ith emission transition dipole. Assuming that each $I^i(t)$ differs from each other by a fractional intensity factor f_i associated with the ith emission transition dipole, Eq. 12 then reduces to

$$I_{\parallel}(t) = (1/3)I(t)\,(1 + 2\sum_i f_i r_i(t)) \tag{13}$$

Because we are only considering one species of fluorophores with many possible emission transition dipoles we can represent $r_i(t)$ as

$$r_i(t) = r^T_{oi} S_i^2 \exp(-t/\phi_p) \tag{14}$$

where it is assumed that the system has an overall rotational correlation time of ϕ_p and that the rotational correlation time of the fluorophore on the macromolecule, ϕ_w, satisfies $\phi_w \ll \phi_p$ so that the double exponential representation of $r(t)$ (Eq. 4) reduces to a single exponential (Eq. 5). This gives rise to a pre-exponential factor similar to that discussed for r_o^{eff} of Eq. 6; that is, r^T_{oi} is the true initial anisotropy resulting from the ith emission transition dipole and S_i^2 is the order parameter squared due to fast nuclear motion of the fluorophore. Substituting Eq. 14 into Eq. 13 gives

$$I_{\parallel}(t) = (1/3)I(t)\,(1 + 2r_o^{eff}\exp(-t/\phi_p)) \tag{15}$$

where

$$r_o^{eff} = \sum_i f_i r^T_{oi} S_i^2 \tag{16}$$

from which S_c^2 is then given by Eq. 9 and can be compared with the experimentally derived S^2 of Eq. 6 provided we solve for f_i using Eq. 10.

APPENDIX B

On the radiative decay of a multi-exponential decaying system

The following discussion is derived from Prof. Gregorio Weber's lecture notes. Let us consider a heterogeneous population of fluorophores each of which decays as a single exponential. The ith fluorophore has a lifetime τ_i with a quantum yield q_i defined by

$$q_i = \frac{k_{ri}}{k_{ri} + k_{nri}} \tag{17}$$

where k_{ri} is the radiative decay rate and k_{nri} is the nonradiative decay rate of the ith species. Let us assume, for simplicity, that $k_{ri} = k_r$. In other words, all species have the same radiative decay rate. Furthermore, let n_i denote the concentration of ith molecular species excited. Then the fractional intensity weighted average lifetime, $\langle\tau\rangle$, is given by

$$\langle\tau\rangle = \sum_i \tau_i n_i q_i \Big/ \sum_i n_i q_i \tag{18}$$

Because $\tau_i = q_i/k_r$ Eq. 18 becomes

$$k_r\langle\tau\rangle = \sum_i n_i q_i^2 \Big/ \sum_i n_i q_i \tag{19}$$

With the average quantum yield $\langle q\rangle$ defined by

$$\langle q\rangle = \sum_i n_i q_i \Big/ \sum_i n_i \tag{20}$$

we redefine q_i as

$$q_i = \langle q\rangle + \delta q_i \tag{21}$$

Using Eq. 21 it follows from Eq. 20 that

$$\sum_i n_i \delta q_i = 0 \tag{22}$$

Applying Eqs. 21 and 22 to Eq. 19 gives

$$k_r\langle\tau\rangle = \langle q\rangle + \sum_i n_i \delta q_i^2/\langle q\rangle \tag{23}$$

The second term on the right hand side of Eq. 23 is always positive and it follows that

$$\langle q\rangle \le k_r\langle\tau\rangle \tag{24}$$

where the equality of Eq. 24 holds for a system that decays as a single exponential; otherwise the inequality holds. $\langle q\rangle$ and $\langle\tau\rangle$ can be obtained experimentally so that we can calculate the experimentally recovered radiative decay rate k_r^{exp} given by

$$k_r^{exp} = \langle q\rangle/\langle\tau\rangle \tag{25}$$

Thus Eq. 24 can be recast as

$$(k_r^{exp})^{-1} \ge (k_r)^{-1} \tag{26}$$

Which states to us a warning: if you have a multiexponential decay then your experimentally recovered radiative lifetime, using Eq. 25, may be larger than the true radiative lifetime.

REFERENCES

Albers, M. W., C. T. Walsh, and S. L. Schreiber. 1990. Substrate specificity for the human rotamase FKBP: a view of FK506 and rapamycin as leucine-(twisted amide)-proline mimics. *J. Org. Chem.* 55:4984–4986.

Alcala, J. R., E. Gratton, and F. G. Prendergast. 1987. Interpretation of fluorescence decays in proteins using continuous lifetime distributions. *Biophys. J.* 51:925–936.

Bajzer, Z., and F. G. Prendergast. 1993. A model for multiexponential tryptophan fluorescence intensity decay in proteins. *Biophys. J.* 65: 2313–2323.

Bajzer, Z., A. Zelic, and F. G. Prendergast. 1995. Analytical approach to the recovery of short fluorescence lifetimes from fluorescence decay curves. *Biophys. J.* 69:1148–1161.

Becker, J. W., J. Rotonda, B. M. McKeever, H. K. Chan, A. I. Marcy, G. Wiederrecht, J. D. Hermes, and J. P. Springer. 1993. FK-506-binding protein: Three-dimensional structure of the complex with the antagonist L-685,818. *J. Biol. Chem.* 268:11335–11339.

Beechem, J. M., and L. Brand. 1985. Time-resolved fluorescence of proteins. *Annu. Rev. Biochem.* 53:43–71.

Beechem, J. M., and E. Gratton. 1988. Fluorescence spectroscopy data analysis environment: a second generation global analysis program. *Proc. SPIE.* 909:70–81.

Bierer, B. E., P. S. Mattila, R. F. Standaert, L. A. Herzenberg, S. J. Burakoff, G. Crabtree, and S. L. Schreiber. 1990. Two distinct signal transmission pathways in T lymphocytes are inhibited by complexes formed between an immunophilin and either FK506 or rapamycin. *Proc. Natl. Acad. Sci. USA.* 87:9231–9235.

Brooks, C. L., R. E. Bruccoleri, B. D. Olafson, D. J. States, S. Swaminathan, and M. Karplus. 1983. CHARMM: a program for macromolecular energy, minimization and dynamics calculations. *J. Comp. Chem.* 4:187–217.

Brown, E. J., M. W. Albers, T. B. Shin, K. Ichikawa, C. T. Keith, W. S. Lane, and S. L. Schreiber. 1994. A mammalian protein targeted by G1-arresting rapamycin-receptor complex. *Nature.* 369:756–758.

Cheng, J. W., C. A. Lepre, S. P. Chambers, J. R. Fulghum, J. A. Thomson, and J. M. Moore. 1993. ^{15}N NMR relaxation studies of the FK506 binding protein: backbone dynamics of the uncomplexed receptor. *Biochemistry.* 32:9000–9010.

Cheng, J. W., C. A. Lepre, and J. M. Moore. 1994. ^{15}N NMR relaxation studies of the FK506 binding protein: dynamic effects of ligand binding and implications for calcineurin recognition. *Biochemistry.* 33: 4093–4100.

Clipstone, N. A., and G. R. Crabtree. 1992. Identification of calcineurin as a key signaling enzyme in T-lymphocyte activation. *Nature.* 357: 695–697.

Demas, J. N., and G. A. Crosby. 1971. The measurement of photoluminescence quantum yields. A review. *J. Phys. Chem.* 75:991–1024.

Egan, D. A., T. M. Logan, H. Liang, E. Matayoshi, S. W. Fesik, and T. F. Holzman. 1993. Equilibrium denaturation of recombinant human FK binding protein in urea. *Biochemistry.* 32:1920–1927.

Fischer, S., S. Michnick, and M. Karplus. 1993. A mechanism for the rotamase catalysis by the FK506 binding protein (FKBP). *Biochemistry.* 32:13830–13837.

Frauenfelder, H., F. Parak, and R. D. Young. 1988. Conformational substates in proteins. *Annu. Rev. Biophys. Biophys. Chem.* 17:451–479.

Frauenfelder, H., S. G. Sligar, and P. G. Wolynes. 1991. The energy landscapes and motions of proteins. *Science.* 254:1598–1603.

Griffith, J. P., J. L. Kim, E. E. Kim, M. D. Sintchak, J. A. Thomson, M. J. Fitzgibbon, M. A. Fleming, R. R. Caron, K. Hsiao, and M. A. Navia. 1995. X-ray structure of calcineurin inhibited by the immunophilin-immunosuppressant FKBP12-FK506 complex. *Cell.* 82:507–522.

Harding, M. W., A. Galat, D. E. Uehling, and S. L. Schreiber. 1989. A receptor for the immunosuppressant FK506 is a *cis-trans* peptidyl-prolyl isomerase. *Nature.* 341:758–760.

Harris, D. L., and B. S. Hudson. 1990. Photophysics of tryptophan in bacteriophage T4 lysozymes. *Biochemistry.* 29:5276–5285.

Harrison, R. K., and R. L. Stein. 1990. Substrate specificities of the peptidyl prolyl *cis-trans* isomerase activities of cyclophilin and FK-506 binding protein: evidence for the existence of a family of distinct enzymes. *Biochemistry.* 29:3813–3816.

Haydock, C. 1993. Protein side chain rotational isomerization: a minimum perturbation mapping study. *J. Chem. Phys.* 98:8199–8214.

Hutnik, C. M., and A. G. Szabo. 1989. Confirmation that multiexponential fluorescence decay behavior of holoazurin originates from conformational heterogeneity. *Biochemistry.* 28:3923–3934.

Janes, S. M., G. Holtom, P. Ascenzi, M. Brunori, and R. M. Hochstrasser. 1987. Fluorescence and energy transfer of tryptophans in aplysia myoglobin. *Biophys. J.* 51:653–660.

Kemple, M. D., P. Yuan, K. E. Nollet, J. A. Fuchs, N. Silva, and F. G. Prendergast. 1994. ^{13}C NMR and fluorescence anisotropy measurements of tryptophan dynamics in wild-type and two single-tryptophan variants of *Escherichia coli* thioredoxin. *Biophys. J.* 66:2111–2126.

Lakowicz, J. R. 1983. Instrumentation for fluorescence spectroscopy. *In* Principles of fluorescence spectroscopy. Plenum Press, New York. 44.

Lakowicz, J. R., B. P. Maliwal, H. Cherek, and A. Balter. 1983. Rotational freedom of tryptophan residues in proteins and peptides. *Biochemistry.* 22:1741–1752.

Lepre, C. A., J. W. Cheng, and J. M. Moore. 1993. Dynamics of a receptor-bound ligand by heteronuclear NMR:FK506 bound to FKBP-12. *J. Am. Chem. Soc.* 115:4929–4930.

Liu, J., J. D. Farmer, Jr., W. S. Lane, J. Friedman, I. Weissman, and S. L. Schreiber. 1991. Calcineurin is a common target of cyclophilin-cyclosporin A and FKBP-FK506 complexes. *Cell.* 66:807–815.

Marquis-Omer, D., G. Sanyal, D. B. Volkin, A. I. Marcy, H. K. Chan, J. A. Ryan, and C. R. Middaugh. 1991. Stabilization of the FK506 binding protein by ligand binding. *Biochem. Biophys. Res. Commun.* 179: 741–748.

McKinnon, A. E., A. G. Szabo, and D. R. Miller. 1977. The deconvolution of photoluminiscence data. *J. Phys. Chem.* 81:1564–1567.

Michnick, S. W., M. K. Rosen, T. J. Wandless, M. Karplus, and S. L. Schreiber. 1991. Solution structure of FKBP, a rotamase enzyme and receptor for FK506 and rapamycin. *Science.* 252:836–839.

Momany, F. A., and R. Rone. 1992. Validation of the general purpose QUANTA3.2/CHARMm force field. *J. Comp. Chem.* 13:888–900.

Moore, J. M., D. A. Peattie, M. J. Fitzgibbon, and J. A. Thomson. 1991. Solution structure of the major binding protein for the immunosuppressant FK506. *Nature.* 351:248–250.

Munro, I., I. Pecht, and L. Stryer. 1979. Subnanosecond motions of tryptophan residues in proteins. *Proc. Natl. Acad. Sci. USA.* 76:56–60.

O'Connor, D. V., and D. Phillips. 1984. Time-correlated Single Photon Counting. 1st ed. Academic Press, New York.

Orozco, M., J. Tirado-Rives, and W. L. Jorgensen. 1993. Mechanism for the rotamase activity of FK506 binding protein from molecular dynamics simulations. *Biochemistry.* 32:12864–12874.

Palmer, A. G., III, R. A. Hochstrasser, D. P. Millar, M. Rance, and P. E. Wright. 1993. Characterization of amino acid side chain dynamics in zinc-finger peptide using ^{13}C NMR spectroscopy and time-resolved fluorescence spectroscopy. *J. Am. Chem. Soc.* 115:6333–6345.

Pang, Y.-P., N. D. Silva, C. Haydock, and F. G. Prendergast. Docking studies of FKBP with its ligands: An induced-fit mechanism in the binding of FKBP. *In* QSAR and Molecular Modeling. In press.

Park, S. T., R. A. Aldape, O. Futer, M. T. DeCenzo, and D. J. Livingston. 1992. PPIase catalysis by human FK506-binding protein proceeds through a conformational twist mechanism. *J. Biol. Chem.* 267: 3316–3324.

Rasmussen, B. F., A. M. Stock, D. Ringe, and G. A. Petsko. 1992. Crystalline ribonuclease A loses function below the dynamical transition at 220K. *Nature.* 357:423–424.

Rayner, D. M., and A. G. Szabo. 1978. Time resolved fluorescence of aqueous tryptophan. *Can. J. Chem.* 56:743–745.

Ruggiero, A. J., D. C. Todd, and G. R. Fleming. 1990. Subpicosecond fluorescence anisotropy studies of tryptophan in water. *J. Am. Chem. Soc.* 112:1003–1014.

Saito, I., H. Sugiyama, A. Yamamoto, S. Muramatsu, and T. Matsuura. 1984. Photochemical hydrogen-deuterium exchange reaction of tryptophan. The role in non-radiative decay of singlet tryptophan. *J. Am. Chem. Soc.* 106:4286–4287.

Schevitz, R. W., N. J. Bach, D. G. Carlson, N. Y. Chirgadze, D. K. Clawson, R. D. Dillard, S. E. Drahmeim, L. W. Hartley, N. D. Jones, E. D. Mihelich, J. L. Olkowski, D. W. Snyder, C. Sommers, and J.-P. Wery. 1995. Structure-base design of the first potent and selective inhibitor of human non-pancreatic secretory phospholipase A_2. *Nature Struct. Biol.* 2:458–465.

Schreiber, S. L. 1992. Immunophilin-sensitive protein phosphatase action in cell signaling pathways. *Cell.* 70:365–368.

Schreiber, S. L., and G. R. Crabtree. 1992. The mechanism of action of cyclosporin A and FK506. *Immunol. Today.* 13:136–142.

Sharp, K. A. 1993. Inclusion of solvent effects in molecular mechanics force fields. *In* Computer Simulation of Biomolecular Systems. Theoretical and Experimental Applications. Vol. 2. W. F. Gunsteren, P. K. Weiner, and A. J. Wilkinson, editors. ESCOM, Leiden. 147–160.

Shizuka, H., M. Serizawa, T. Shimo, I. Saito, and T. Matsuura. 1988. Fluorescence-quenching mechanism of tryptophan. Remarkably efficient internal proton-induced quenching and charge-transfer quenching. *J. Am. Chem. Soc.* 110:1930–1934.

Siekierka, J. J., S. H. Y. Hung, M. Poe, C. S. Lin, and N. H. Sigal. 1989. A cytosolic binding protein for the immunosuppressant FK506 has peptidyl-prolyl isomerase activity but is distinct from cyclophilin. *Nature.* 341:755–757.

Sigal, N. H., and F. J. Dumont. 1992. Cyclosporin A, FK-506 and rapamycin: pharmacologic probes of lymphocyte signal transduction. *Annu. Rev. Immunol.* 10:519–560.

Starzl, T. E. 1993. FK506 versus cyclosporine. *Transplant. Proc.* 25: 511–512.

Starzl, T. E., J. Fung, M. Jordan, R. Shapiro, A. Tzakis, J. McCauley, J. Johnston, Y. Iwaki, A. Jain, M. Alessiani, and S. Todo. 1990. Kidney transplantation under FK506. *JAMA.* 264:63–67.

Steiner, R. F., and E. P. Kirby. 1969. The interaction of the ground and excited states of indole derivatives with electron scavengers. *J. Phys. Chem.* 73:4130–4135.

Szabo, A. G., and C. Faerman. 1992. Dilemma of correlating fluorescence quantum yields and intensity decay times in single tryptophan mutant proteins. *SPIE, Time-Resolve Laser Spectroscopy in Biochemistry III.* 1640:70–80.

Thomson, A. W. 1989. FK-506—how much potential? *Immunol. Today.* 10:6–9.

Valeur, B., and G. Weber. 1977. Resolution of the fluorescence excitation spectrum of indole into the ^1L_a and ^1L_b excitation bands. *Photochem. Photobiol.* 25:441–444.

Van Duyne, G. D., R. F. Standaert, P. A. Karplus, S. L. Schreiber, and J. Clardy. 1991a. Atomic structure of FKBP-FK506, an immunophilin-immunosuppressant complex. *Science.* 252:839–842.

Van Duyne, G. D., R. F. Standaert, S. L. Schreiber, and J. Clardy. 1991b. Atomic structure of the rapamycin human immunophilin FKBP-12 complex. *J. Am. Chem. Soc.* 113:7433–7434.

van Gunsteren, W. F., and M. Karplus. 1980. A method for constrained energy minimization of macro molecules. *J. Comp. Chem.* 1:266–274.

Verlinde, C. L. M. J., and B. W. Dijkstra. 1995. Drug or tool, design or serendipity? *Nature Struct. Biol.* 2:429–432.

Wetlaufer, D. B. 1962. Ultraviolet absorption spectra of proteins and amino acids. *Adv. Protein Chem.* 17:303–390.

Wiederrecht, G., S. Hung, H. K. Chan, A. Marcy, M. Martin, J. Calaycay, D. Boulton, N. Sigal, R. L. Kincaid, and J. J. Siekierka. 1992. Characterization of high molecular weight FK-506 binding activities reveals a novel FK-506-binding protein as well as a protein complex. *J. Biol. Chem.* 267:21753–21760.

Wilson, K. P., M. M. Yamashita, M. D. Sintchak, S. H. Rotstein, M. A. Murcko, J. Boger, J. A. Thomson, M. J. Fitzgibbon, J. R. Black, and M. A. Navia. 1995. Comparative x-ray structures of the major binding protein for the immunosuppressant FK506 (tacrolimus) in unliganded form and in complex with FK506 and rapamycin. *Acta Crystallogr.* D51:511–521.

Yamamoto, Y., and J. Tanaka. 1972. Polarized absorption of spectra of crystals of indole and its related compounds. *Bull. Chem. Soc. Jpn.* 45:1362–1366.

Yu, N. T. 1977. Raman spectroscopy: a conformational probe in biochemistry. *CRC Crit. Rev. Biochem.* 4:229–280.